







Generation of annular femtosecond few-cycle pulses by self-compression and spatial filtering in solid thin plates

YITAN GAO,^{1,2}  YABEI SU,^{1,3} SIYUAN XU,^{1,3} XIAOXIAN ZHU,^{1,2}
KUN ZHAO,^{1,4,5}  SHAOBO FANG,^{1,2,4} JIANGFENG ZHU,³  AND
ZHIYI WEI^{1,2,4,6} 

¹Beijing National Laboratory for Condensed Matter Physics, Institute of Physics, Chinese Academy of Sciences, Beijing 100190, China

²University of Chinese Academy of Sciences, Beijing 100049, China

³School of Physics and Optoelectronic Engineering, Xidian University, Xi'an 710071, China

⁴Songshan Lake Materials Laboratory, Dongguan 523808, China

⁵zhaokun@iphy.ac.cn

⁶zywei@iphy.ac.cn

Abstract: Annular-shaped femtosecond few-cycle pulses are generated by 40fs laser pulses propagating through 6 solid thin plates in numerical simulations as well as in experiments. The generation of such pulses takes advantage of the conical emission caused by plasma effect, which introduces continuously varying off-axis plasma density along the radial direction of the propagating beam. The negative dispersion induced by the plasma causes the pulse at particular radial location to be self-compressed and to form an annular beam of short pulse, which can be extracted simply by spatial filtering. Meanwhile, by adjusting the input pulse energy and position of each thin plate relative to the laser focus, we control the plasma density in thin plates which changes the ratio between ionization and effects providing positive dispersion, and obtain a higher compression ratio indicating that the scheme of solid thin plates has the flexibility to regulate the laser intensity so as to plasma density, thus the negative dispersion the pulse experiences during propagation. Few-cycle pulses as short as 8.8 fs are generated in experiments, meanwhile the shortest pulse duration found in the simulations is 5.0 fs, which corresponds to two optical cycles at its central wavelength 761 nm. This method has great potential in high-power few-cycle pulse generation.

© 2021 Optical Society of America under the terms of the [OSA Open Access Publishing Agreement](#)

1. Introduction

Self-compression is a common phenomenon in strong femtosecond laser propagation in nonlinear media [1–4]. It is a complex process, in which a number of linear and nonlinear effects are involved. Generally, self-compression occurs when the effects providing positive dispersion to the laser pulses balance with the ones providing negative dispersion. The role of material dispersion in self-compression depends on the wavelength of the input pulses. A large number of relevant researches which studied the mechanism of self-compression in gases usually worked in the region where the medium had negative dispersion in the wavelength range of the input pulses, which was able to balance the positive dispersion induced by Kerr effect [5,6]. If the medium has positive dispersion, some laser-induced effect would be necessary to provide negative dispersion for self-compression to take place. For input pulses with wavelength around 800nm where material usually has positive dispersion, the longer wavelength components move faster while the shorter wavelength components stay behind during the propagation. However, taking the nonlinear effects the pulse experiences into account, the chirp evolution of the pulse becomes more complicated. Self-phase modulation (SPM) produces extra longer wavelength components

near the front edge of the pulse, and extra shorter wavelength near the trailing edge. It is similar to positive dispersion or positive index of refraction change the pulse experiences when traveling in normal dispersion material. For plasma effect, it functions in the back of the pulse because material is usually ionized at the leading edge and the plasma gathers at the trailing edge. Then the negative refractive index produced by plasma pushes the shorter wavelength components in the trailing edge forward, which is similar to negative dispersion. Meanwhile, the self-steepening effect also exists, which slows down the propagation of the back part of the pulse. Therefore, under the influence of all the effects mentioned above, supercontinuum generation, self-compression as well as pulse splitting occur together during the propagation.

In previous researches, high order nonlinearity as well as ionization have been identified as major negative index of refraction contributors. Taking advantage of such contributors, self-compression results have been achieved [4,7–12]. Theoretical works about the effects of ionization in self-compression have also been carried out, predicting that there existed a range of plasma density most effective for self-compression [13]. Meanwhile, self-compression has also been observed in hollow-core fibers, which was contributed to a combination of ionization-induced spectral broadening, plasma-induced change of refractive index, and waveguide effect [7,14–18]. In solid-state materials, the mechanism of self-compression is similar as it in gas, but the characteristic parameters for dispersion, Kerr effect as well as photon ionization are much larger than those in gases. It is worth noting that SPM is adverse towards self-compression in normal dispersion material, because it introduces positive dispersion, while plasma provides effect equivalent to negative dispersion, which compresses the pulse. However, SPM provides new spectral components together with ionization spectral broadening, which is necessary for broader spectra to support shorter pulses. Therefore, dispersion matching for self-compression is about balancing all the linear and nonlinear effects along the propagation. Unfortunately, dispersion matching in solids is more sensitive and delicate, and needs to be precisely controlled in order to achieve high rate of self-compression, otherwise pulse splitting forms easily.

Besides, the regulations of optical parameters in solid material itself are also hard to realize. When we apply conventional nonlinear materials in self-compression experiments, what we can do in controlling strength of nonlinear effects are thickness changing and position relocating. However, unlike in gases, where pressure gradient operation is commonly employed to suppress multiple filamentation in self-compression [19], it is impossible to change the solid density to avoid too much undesired ionization. Therefore, it is difficult to optimize self-compression processes in solids. Although it has been alleviated by introducing pre-chirped rather than transform-limited input pulses [20], generating self-compressed pulses through solid medium is much harder in experiments. Fortunately, scheme of multiple thin plates as a novel method has been widely applied in spectral broadening and few-cycle pulse generation in recent years [21,22]. Its unique structure has advantages in generating high-energy few-cycle pulses, while self-compression, relying on plasma generation to provide negative dispersion, also has the ability to bear high energy. Applying self-compression technique in solid thin plates has enormous potential in high-energy few-cycle pulse generation. Moreover, using multiple thin plates is capable of eliminating filamentation by adjusting the location of each plate relative to the laser focal point, which is beneficial in preserving the coherence of newly generated pulses with broader spectra.

To this end, we numerically simulate the self-compression process of femtosecond pulses propagating through solid thin plates. By adjusting the location of each plate relative to the input laser focus, we introduce suitable ionization in the plates so that the negative dispersion brought in by plasma matches the positive dispersion involved in the entire propagation. Furthermore, in consideration of the output Bessel-like beam of the thin plates which is caused by conical emission, we use spatial filtering to select self-compressed hollow pulses in order to avoid pulse splitting easily generated along the propagation axis. In our simulation, few-cycle hollow-pulse

generation via self-compression is realized by spatial mode selection for the first time, which provides a unique method for searching and optimizing self-compressed pulses spectrally as well as spatially. Meanwhile, we successfully obtain self-compressed hollow pulses experimentally. The measurement shows 8.8 fs annular pulses are generated directly by a set of solid thin plates, which confirms the feasibility of utilizing conical emission in self-compression. This method provides a new route in high-energy few-cycle pulse generation.

2. Principle

2.1. Conical emission in thin plates

Conical emission is a common phenomenon when strong laser pulses propagate in medium [23,24]. This angular emission of anti-Stokes-shifted radiation appears when filamentation occurs, and experimental and numerical investigations have already proved plasma generation to be one of the main factors resulting in rainbow ring structures [25–27]. Generally, when describing laser pulse propagation, plane wave approximation is applied to simplify the calculations, and the wave vector is considered in z direction only. However, in the investigation of angular emission, the transverse wave vector needs to be considered, so the wave vector of axially symmetric wave front is given by $\vec{k} = k_z \hat{z} + k_r \hat{r}$, while k_z and k_r are the axial and radial components, respectively. During propagation, both components are affected by the nonlinear effects that the pulse experiences. When intense laser pulses enter the medium, the variation of the wave vector is

$$\Delta \vec{k} = -\frac{\omega_0 \Delta n}{c} \hat{k} = \left(-\frac{\omega_0}{c} n_2 \int_0^t \frac{\partial I}{\partial t} dt + \frac{2\pi e^2}{m_e \omega_0} \int_0^t \frac{\partial \rho}{\partial t} dt \right) \hat{k}, \quad (1)$$

where $\hat{k} = \frac{\vec{k}_0}{|\vec{k}_0|} = \frac{k_{z0} \hat{z} + k_{r0} \hat{r}}{\sqrt{k_{z0}^2 + k_{r0}^2}}$ is the unit vector of the initial wave vector and Δn includes the influence of Kerr effect $\Delta n_{\text{kerr}} = n_2 I(t)$ and plasma induced effect $\Delta n_{\text{plasma}} = -\frac{2\pi e^2 \rho(t)}{m_e \omega_0^2}$. Here n_2 is the nonlinear refractive index of the material, $\rho(t)$ is the plasma density as a function of time, e and m_e are the charge (positive value) and mass of electron, ω_0 is the center angular frequency, and c is the speed of light in vacuum. It is clear that Δn_{kerr} is proportional to laser intensity I while Δn_{plasma} is proportional to a higher power of I , which means plasma effect is more sensitive to laser intensity than Kerr effect. Obviously, the axial component is $\Delta k_z = -\frac{\omega \Delta n}{c} \frac{k_{z0}^2}{\sqrt{k_{z0}^2 + k_{r0}^2}} = -\frac{\omega \Delta n}{c} \frac{k_{z0}}{k_0}$

and the radial component $\Delta k_r = -\frac{\omega \Delta n}{c} \frac{k_{r0}}{k_0}$. The radial or transverse component results in a spatial divergence of laser pulse, especially under the ionization condition which provides a positive Δk_r to push the vector away from the propagation axis. The expression of the wave vector indicates that the spatial divergence is affected by the plasma density that pulse experiences, and it is the prevailing factor because plasma generation is proportional to a higher power of the laser intensity. During the pulse propagation, the trailing edge of the pulse passes through the plasma produced by the front edge, a high plasma density reinforces the divergence, and the blue-shifted part of the spectrum generally has a larger divergence angle, so that the colorful rings of conical emission distribute outward along the radial direction from long to short wavelengths.

In most cases, conical emission is unpopular in few-cycle pulse generation, because it is responsible for energy loss and pulse distortion, but for self-compression, conical emission could be advantageous. Pulse components at different divergence angles caused by conical emission experience different dispersion. Near the propagation axis, the beam has high intensity so that both Kerr and plasma effects contribute. However, the nonlinear effects usually do not match the material dispersion exactly, and pulse splitting always happens in strong laser fields. Relevant researches about self-compression in solid are normally restrained with low pulse energy [28].

However, in contrast with the on-axis part, the divergent part of the laser beam caused by conical emission experiences different strength of nonlinear effects. When conical emission occurs, the divergent part deviates from the peak intensity area so that less nonlinear effects are involved. The nonlinear effects as well as the plasma density along the divergent path may be estimated by the pulse intensity distribution of every single moment during propagation. In consideration of the plasma induced negative dispersion, different paths experience differently, which means the angular divergence may be taken advantage to balance the dispersion. Finally, the negative dispersion variation caused by the plasma distribution in the spatial beam profile differentiates the transverse wave vector $\Delta k_r \hat{r}$ spatially. Therefore, unlike the difficult dispersion control along the propagation axis, spatial filtering is able to find a more precise route for dispersion matching in the ring structures generated by conical emission for self-compression. (Fig. 1)

From the output beam profile of thin plates, the colorful rings have also been observed, although thin plates is able to effectively reduce the filamentation inside solid material [22]. This means conical emission is sensitive to ionization and is formed even in low plasma density. Meanwhile, the scheme of thin plates is able to control the laser intensity in each plate, and the plasma density as well. By combining the advantages of conical emission and thin plates, precise regulation of the plasma density may be realized since the laser intensity as well as the plasma density vary continuously along the radial direction. Such plasma density control as well as negative dispersion control, to some extent, are reflected at the spatial distribution of the output beam. Therefore, based on conical emission of thin plates, self-compressed pulse may be achieved by spatial filtering.

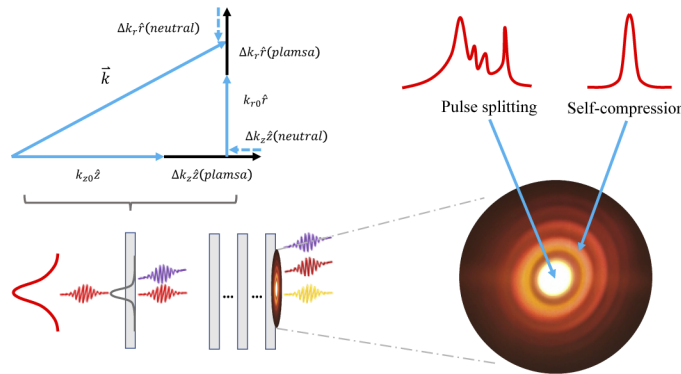


Fig. 1. The schematic diagram of annular beam formation and its benefit in self-compression. From left to right, principle of conical emission in solid thin plates is shown, the transverse wave vector $k_r \hat{r} = k_{r0} \hat{r} - \Delta k_r \hat{r}(\text{neutral}) + \Delta k_r \hat{r}(\text{plasma})$ causes beam to diverge, and form colorful Bessel-like beam structure which is from the interference of conical emission in multiple plates. The transverse wave vector changes continuously along the radial direction due to the variable spatial gradient of plasma density generated by the laser pulse. Different divergence angles represent different degree of ionization, introducing different negative dispersion.

2.2. Pulse propagation model of self-compression

To simulate self-compression process in thin plates, we employ a time-dependent nonlinear Schrödinger equation (TDNSE) as in Eq. 2, which describes a forward propagating pulse going through different linear and nonlinear effects during laser-matter interaction, including diffraction, group velocity dispersion (GVD), third order dispersion (TOD), optical Kerr effect, plasma induced refractive index change, multiphoton absorption and collision ionization [29,30].

The plasma formation is calculated by the multiphoton-ionization equation, which specifies the generated plasma density ρ (same as in Eq. 1) under the consideration of free electron recombination (Eq. 3).

$$\partial_z U = \frac{i}{2k_0} T^{-1} \nabla_{\perp} U + i D U + i \frac{\omega_0}{c} n_2 T U - i \frac{k_0}{2n_0 \rho_c} T^{-1} \rho U - \frac{\beta^{(\kappa)}}{2} |U|^{2\kappa-2} U - \frac{\sigma}{2} \rho U, \quad (2)$$

$$\frac{\partial \rho}{\partial t} = W_I (|U|^2) + \frac{\sigma \rho |U|^2}{U_i} - \frac{\rho}{\tau_{rec}}. \quad (3)$$

The normalized envelope $U(r, t, z)|_{z=0} = e^{(-r^2/R^2 - t^2/\tau^2)} \cdot F_{\text{lens}}$, where $F_{\text{lens}} = e^{(-ik_0 r^2/2f)}$ represents the phase change by the focusing lens of the input beam. In the wave vector amplitude $k_0 = n_0 \omega_0 / c$, n_0 is the linear refractive index of the spectral broadening material, namely the thin plates. The nonlinear refractive index for fused silica is $n_2 = 2.4 \times 10^{-14} \text{ mm}^2/\text{W}$. T and ∇_{\perp} are the spatio-temporal coupling operator and spatial second-order differential operator, respectively. D operator contains the effect of GVD and TOD. Then the following two terms represent the Kerr and plasma induced effects, which cause changes in refractive index. The last two terms are energy loss resulted from photon-ionization. ρ_c is the critical plasma density of the medium. $\beta^{(\kappa)}$ is the coefficient for multiphoton absorption, where $\kappa \equiv 6$. The ionization potential U_i is 9 eV for fused silica, and the cross-section of collisional ionization $\sigma = 6 \times 10^{-18} \text{ cm}^2$ and recombination time $\tau_{rec} = 27 \text{ fs}$. The ionization rate W_I for silica was taken from Keldysh's multiphoton rate. Details of these parameters have been discussed previously [31].

3. Numerical simulations

In our simulation based on Eq. 2, we consider input pulses with parameters of 800 nm, 40 fs, pulse energy ranging from 0.5 to 0.8 mJ, and focused by a 2 m focusing lens (Fig. 1).. There are 6 pieces of fused silica plates placed near the laser focal point. Firstly, we inject pulses with 0.5 mJ energy into the thin plates, which are set at the locations where the widest spectral broadening is obtained. The laser focus is between the 1st and 2nd plates, and the distances between each two plates are around 50 mm. In such a configuration, ionization is partially suppressed to minimize the energy loss, and a supercontinuum pulse is generated. From the simulation, we extract the variation of the pulse envelop along the propagation at different radial locations, as shown in Fig. 2. We also calculate the final output pulse envelopes at different radial locations in air, 100mm downstream from the last plate. Spatiotemporal intensity distributions at five locations in radial direction are plotted in Fig. 2. As we expected, self-compressed pulses are found at $r = 0.3$ and 0.5 mm, which form hollow or annular beams. Pulses both closer to and further away from the propagation axis split, due to dispersion mismatching. Especially on the propagation axis (Fig. 2(a)), a distinct pulse splitting occurs each time the pulse passes through a thin plate because of the strong nonlinearity induced by the high laser intensity. However, as Fig. 2(f) shows, even though a self-compressed pulse is acquired at $r = 0.45$ mm, it is not short enough, whose compression ratio is only 4.3, far from the ideal ratio in solid [32]. The temporal profile is not clean enough either, with a large pedestal and a small post-pulse following. The reason for this is two-fold. First, ionization-induced spectral broadening is not enough so that the spectrum is not wide enough to support shorter pulses. Second, the negative dispersion does not compensate the positive dispersion enough to make the self-compressed pulse close to the Fourier transform limit.

According to this speculation, we therefore increase the input pulse energy to reinforce ionization, which is able to provide a broader spectrum and higher negative dispersion. After raising the pulse energy from 0.5 to 0.8 mJ, we calculate the plasma density in each plate, as

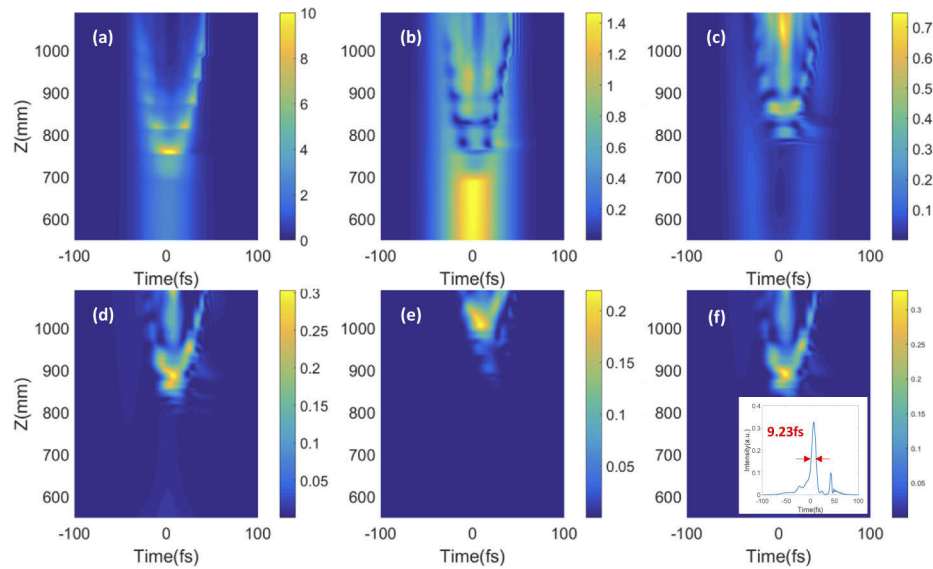


Fig. 2. Temporal profile of the pulse versus propagation distance at different radial positions, (a) $r = 0$, (b) $r = 0.1$ mm, (c) $r = 0.3$ mm, (d) $r = 0.5$ mm, (e) $r = 1$ mm, where the thin plates locate at $z = 650, 710, 770, 830, 890, 950$ mm. Self-compressed pulses are observed at $r = 0.3$ and 0.5 mm which form annular beams. Pulses both closer to ($r = 0$ and 0.1 mm) and further away ($r = 1$ mm) from the propagation axis split. The shortest self-compressed pulse is found at $r = 0.45$ mm, and (f) is the spatial-temporal profile of the shortest pulse that we found. The inset shows the temporal profile of the simulated output pulse, and the duration is 9.2 fs at full-width of half maximum (FWHM), longer than its transform-limited pulse duration 8.0 fs though.

shown in Fig. 3(a). Here we apply average plasma density in whole temporal and spatial range for the purpose of investigating the overall effect of induced plasma. Plasma generation in air is neglected because it is several orders of magnitude lower than that in the plates. Figure 3 also shows the shortest self-compressed pulses at different input pulse energies. At the same time, the radius of the hollow beam of the shortest self-compressed pulse becomes bigger with the increasing of input pulse energy. This observation is consistent with that, as higher plasma density is generated by the laser pulses with higher energy, the dispersion-matched transverse component of the wave vector is pushed further outward. This result indicates that there is always a radial location where self-compressed pulses appear, and rising the input pulse energy increases the self-compression ratio as well. We find self-compressed 6.4 fs pulses under 0.8 mJ input pulse energy (Fig. 3(d)).

From the results shown in Fig. 3, it is clear that the more plasma is generated by higher input energy, the shorter the pulse is compressed. Since negative dispersion of conical emission varies as the radial distance from the propagation axis varies, conical emission produced by higher plasma density means a wider range in the radial direction for us to adjust negative dispersion, which also means a better dispersion-matched pulse is able to be picked up. However, increasing the input power does not guarantee higher plasma density in all the plates, as shown in Fig. 3(a). The highest laser intensity is located at the second plate just like the situation in experiments, while the plasma density under 0.8 mJ pulse energy in the following plates are even lower than 0.5 and 0.6 mJ (except the last one). Obviously, the shortest self-compressed pulse found under 0.8 mJ is better than 0.5 and 0.6 mJ, which means the plasma density of the first two plates plays a dominant role in inducing negative dispersion, and has the possibility in introducing more

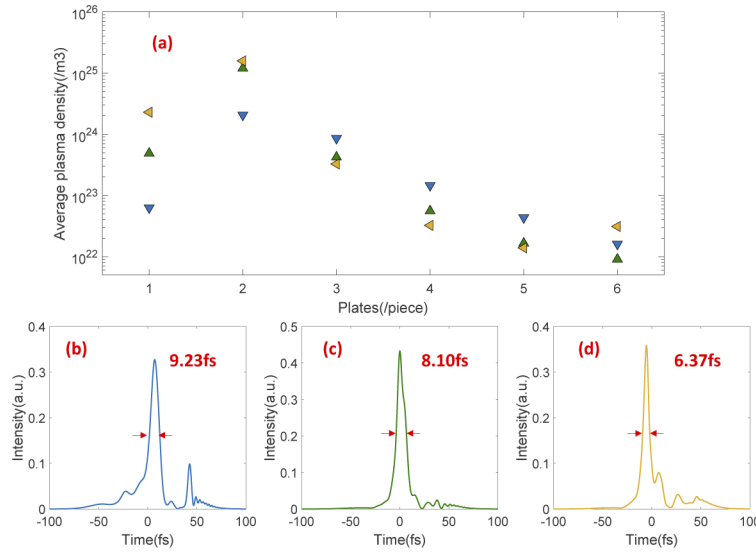


Fig. 3. Self-compression results at different initial pulse energies (all other conditions and positions of the thin plates are the same). (a) Laser-induced plasma density averaged in each thin plate with input energies of 0.5 (blue inverted triangle), 0.6 (green regular triangle), and 0.8 mJ (orange oblique triangle). (b)(c)(d) Temporal profiles of the shortest pulses at 0.5, 0.6 and 0.8 mJ input energies, respectively; and the radial locations of these pulses are 0.45, 0.76, and 0.85 mm away from the propagation axis, respectively (the sampling plane to measure the pulse profiles is in the air, 100 mm after the last plate).

ionization to obtain better dispersion matching. In order to increase overall plasma density in all the plates, we move forward the 1st plate to reduce the beam divergence in the subsequent plates, reduce the distance between the 1st and 2nd plates to maintain a high laser intensity in the entire propagation, and move the rest of plates forward as well. The distance between each plates are reduced to 25mm roughly. Then we calculate the average plasma density of this new configuration (Fig. 4(a)), and find the plasma density is increased significantly. Figure 4(c) shows the spatio-temporal intensity distribution of the output beam. Along the propagation axis, serious pulse splitting occurs, which also indicates a strong spectral broadening. While in the hollow beam at $r = 0.95$ mm, a relatively strong self-compression pulse appears, and the annular pulses at radial positions near $r = 0.95$ mm all have similar temporal profiles, shown as the shadow region of Fig. 4(c). The area further out is a mixture of conical emission from each plate and the diffraction of the input laser beam. In this area, the pulses are mainly composed of high-frequency components, which are mainly generated by the ionization in the trailing edge. These components in this outer skirt of the beam lag behind the pulse in the inner part. Formation of a dynamic multipeak structure is clear in the spatio-temporal distribution of the pulse (Fig. 4(c)), indicating that the angular spectral distribution along with the spectral broadening of the pulse during and after the propagation of laser pulse through the medium reveal ample information about the nonlinear propagation. The spatio-spectral distribution of the output beam illustrates that the blue shift of conical emission dominates the off-axis region, as shown in Fig. 4(d). When we filter out a hollow beam at $r = 0.95$ mm spatially, its temporal profile indicates a pulse duration of 5.0 fs with an excellent pulse contrast and compression ratio of 8.0, and its central wavelength is about 761 nm. Furthermore, we find that the temporal profile of the self-compressed pulse keeps unchanged when we move the beam profile sampling plane downstream 200 mm along the propagation axis to test the temporal stability of the pulse. Such a short hollow pulse is favorable

for applications such as field trapping of atoms and high-order harmonic generation with high power lasers [33]. However, the average plasma density in the second plate is $8.7 \times 10^{25}/\text{m}^3$, very close to the damage threshold $10^{26}/\text{m}^3$ probably due to avalanche ionization, thus we should reduce the laser intensity in the second plate to avoid material damage in subsequent experiments.

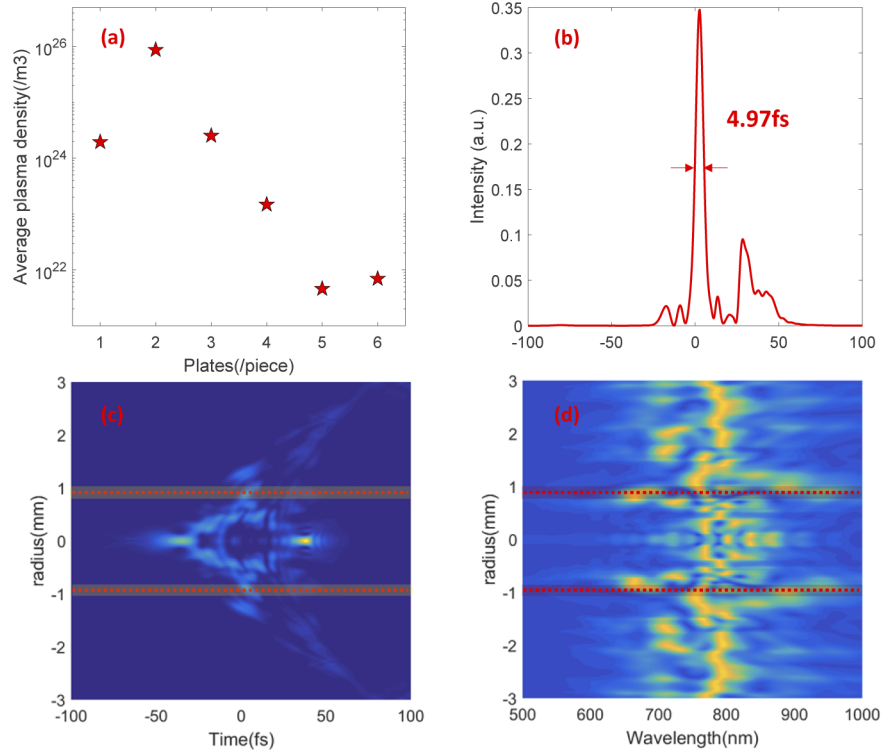


Fig. 4. Adjusting the position of plates at 0.8 mJ input energy to increase the ionization in all the plates. (a) The average plasma density in each plate, where the plasma density of the second plate is clearly increased from the result of 0.8 mJ energy shown in Fig. 3. (b) The temporal profile of the shortest pulse, whose pulse duration is 5.0 fs (FWHM), and the compression factor is as high as 8.0. (c) The spatio-temporal intensity distribution and (d) the spatio-spectral distribution of the output beam (the sampling plane is in the air, 100 mm after the last plate), where the best self-compression pulse appears around $r = 0.95$ mm (red dashed lines), and the width of the radial slice where the pulses generated inside could be considered the same is about 0.3 mm (shadow area).

4. Experimental results and discussion

The self-compressed annular pulses are also generated in experiments, and the results are consistent with our simulations. The 40 fs driving pulses with 790 nm central wavelength are produced at 1 kHz repetition rate by a commercial Ti:sapphire amplifier (Astrella, Coherent Inc.). A telescope constructed with concave mirrors are applied to control the beam diameter and divergence, so that the laser parameters are consistent with those in our simulations. Firstly, under 0.5 mJ input pulse energy, supercontinuum with a Bessel-like shape is formed, followed by a simple spatial filter to produce an annular beam as shown in Fig. 5. Since the whole propagation process is axisymmetric, a small part on the ring reflects the characteristics of the entire annular beam, so a part of the annular beam is selected for pulse temporal measurement. The experimental setup for supercontinuum generation and selection of self-compressed pulses is

shown in Fig. 5. We use a 3:1 telescope to reduce the input beam diameter, and 6 pieces of fused silica thin plates are placed behind a 2m concave mirror. After the thin plates, another concave mirror with same focal length collimates the output beam, then a self-made circular spatial filter is applied to block the center bright spot of the beam. Finally, a diaphragm is used to allow a small part of the first ring of the output beam to enter the D-scan (D-scan B, Sphere Inc.) for pulse duration measurement. The measuring results of self-compressed annular pulses confirm our simulations, as shown in Fig. 6, that a 9.5 fs pulse is generated. Several measurements under similar conditions show the pulse duration stabilizes between 9 and 10 fs. It is worth noting that the position of measuring device is about 1.5 m away from the last plate, and the dispersion of air has been taken into consideration in the measurements.

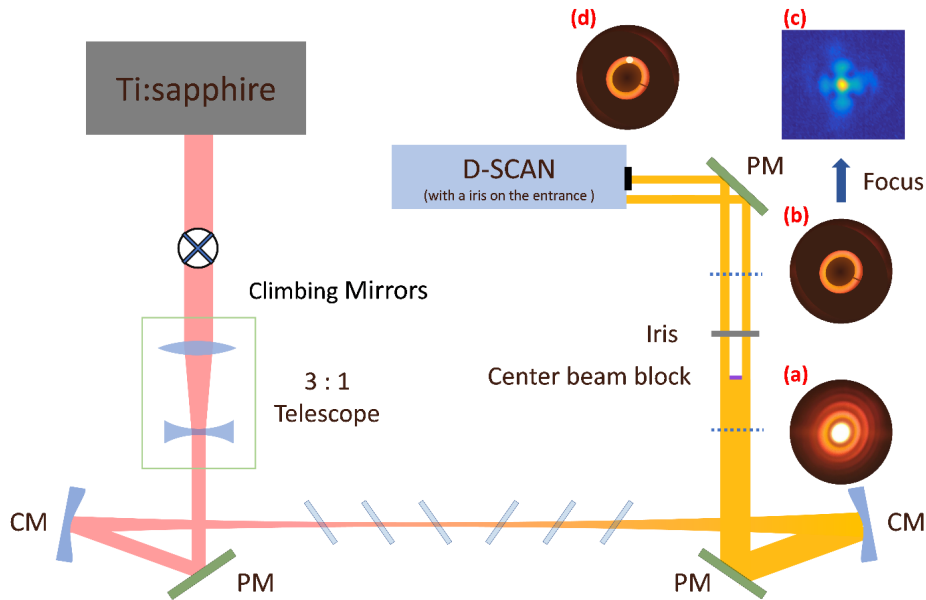


Fig. 5. The experimental schematic diagram of annular self-compression pulse generation based on fused silica thin plates. The spatial beam profiles of spectral broadened laser pulses before and after the spatial filter are taken from real experiments. Ti:sapphire: Ti:sapphire laser amplifier, CM: concave mirror, PM: plane mirror, D-SCAN: dispersion-scan pulse measuring device. The beam profiles: (a) collimated output beam from the thin plates; (b) annular beam after the spatial filters (a center beam block and an iris); (c) focal spot of the annular beam; (d) a diaphragm is used to allow a small part of the annular beam to enter the D-scan.

While searching for the self-compressed pulses, we notice that nearby annular pulses are not well-compressed or not compressed at all, which means the dispersion matching appears only within a very narrow range of experimental parameters as our theoretical model predicts. Besides, the central wavelength of the pulse shown in Fig. 6 is 768 nm, which embodies the characteristics of anti-Stokes Raman emission in conical emission, while the broad bandwidth is mainly induced by SPM in the following plates, as the energy of divergent pulses by conical emission are not intense enough. The structure of thin plates introduces proper amount of ionization as well as negative dispersion in specific plates, and the rest of plates only provide spectral broadening, which is impossible in bulk materials due to its quite narrow spectrum of conical emission [34,35]. Meanwhile, it is the subsequent broadening of the conical emission in the following plates that results in less spatial chirp in the annular beam, which has been proved by spectral measurements

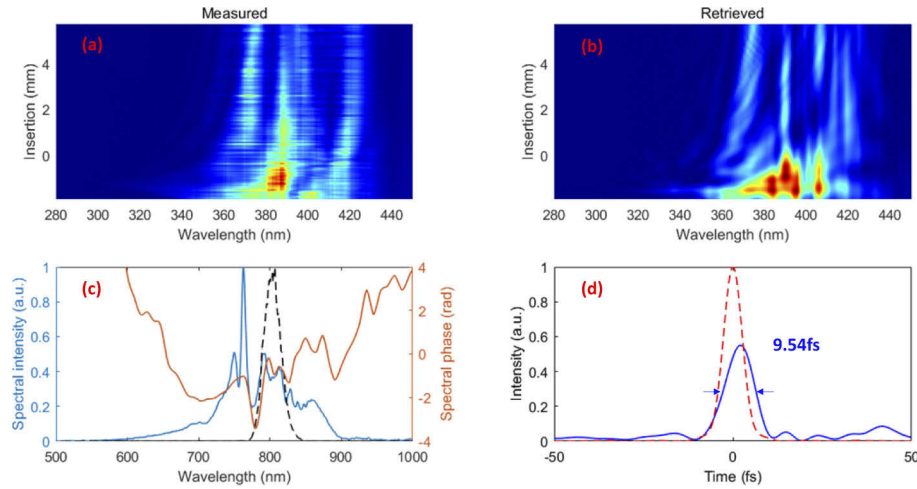


Fig. 6. Characterization of the 9.5 fs pulse by D-SCAN. (a), (b) Measured and retrieved dispersion scan traces. (c) measured input (black dashed line) and output (blue line) spectra, and retrieved spectral phase (red line). (d) temporal intensity profile of the measured pulse envelope (blue line), temporal intensity profile of the transform limited pulse (dashed line). The retrieval error is 0.031.

at different parts of the annular beam in our experiments. Moreover, unlike the dispersed colorful ring of conical emission in a bulk solid plate, the output beam of the thin plates has a Bessel-like shape, and the photons in each ring have similar optical path, similar linear and nonlinear phases so that the spatial chirp in each ring is insignificant. This is why the structure of thin plates has the ability in utilizing conical emission and generating self-compressed annular pulses. When we measure the temporal width of the annular pulses in the experiments, the width of the radial slice included in the measurement is about 2 mm, and the pulse durations and spectra within this 2 mm are about the same. Besides, for the spectra of self-compressed pulses measured along the radial direction as shown in Fig. 7(a), the spectrum of the central ring is slightly wider than those of the inner and outer rings, due to the higher intensity of the best dispersion-matching pulse (the central ring) which induces more nonlinear spectral broadening. Meanwhile, although the spectra of inner and outer rings are somewhat different, the difference is still tolerable as the Fourier transform limits of all these three spectra are about 6 fs. Therefore, the spatial chirp in the annular beam produced by the thin plates is negligible. We note that 2 mm is the smallest diameter of the diaphragm we use in the experiments to send a small part of the beam for pulse duration measurement, and an even smaller diaphragm would not transmit enough energy as required by D-scan to measure the pulse duration.

Whereafter, we try to enhance ionization for better self-compressed pulse generation as the simulation suggests. Unfortunately, the results are not satisfactory. There are two approaches in increasing plasma density. First we optimize the position of thin plates, by moving the first two plates closer to the focus, then adjusting the position of the following plates to ensure a good output beam shape. However, the measured pulse temporal profiles are worse than the results we showed earlier because of the instability of the laser beam caused by too much ionization. The only acceptable result is an 8.8 fs self-compressed annular beam measured with 0.057 retrieval error, while numerical simulation under the same condition predicts a pulse duration of 8.3 fs, as shown in Figs. 7(b) and 7(c). Second, we increase the input laser energy from 0.5 to 0.8 mJ, but the plates are rapidly damaged or the output spectrum is not broader than that at 0.5 mJ, which

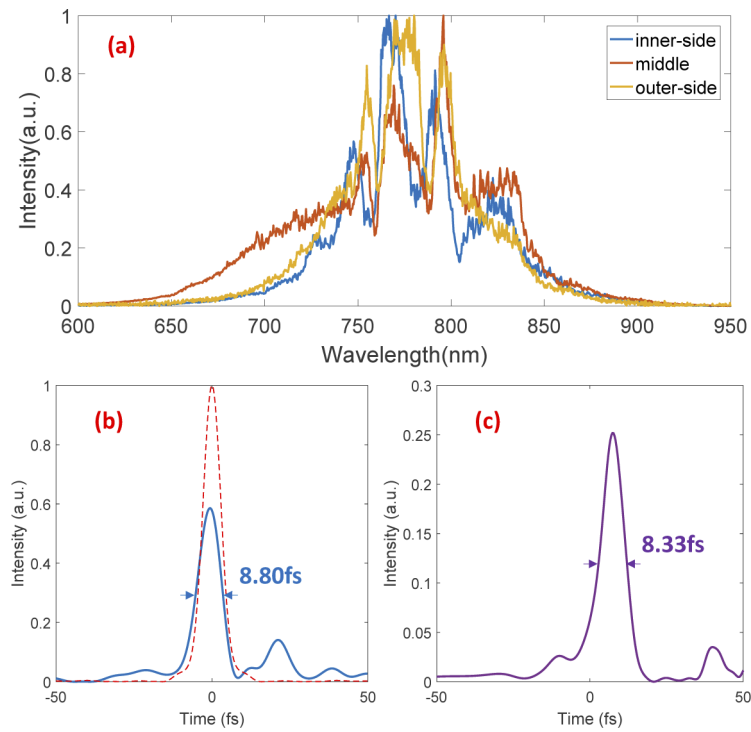


Fig. 7. Spatial chirp in self-compressed annular beam and the temporal profile of the more-ionization induced 8.8 fs pulse measured by D-SCAN and the corresponding simulation result. (a) spectra of different rings in the hollow beam (b) temporal profiles of the measured pulse envelope (blue line) and the transform limited pulse (dashed line) (c) simulated temporal profile under the same pulse propagation condition.

is mainly due to the insufficient focal length. We will optimize the focal parameter and choose plates with higher damage threshold in the following experimental research.

Unfortunately, such a short hollow pulse carries little energy. Because the center peak in the transverse beam profile after the thin plates contains the major part of the total pulse energy, spatial ring-shaped filtering causes inevitably massive energy loss. Unless the central part of the beam is involved, self-compression in solid thin plates would always lead to short but low-energy annular pulses. This drawback may be solved by increasing input energy sufficiently without reaching the threshold of material ionization damage, since solid thin plates has the advantage of being able to take high-energy input pulses. The simulated pulse in Fig. 4(c) has about 40 uJ energy, and the pulse energy of the ~9 fs annular beam in Figs. 6 or 7 is about 30 uJ measured in the experiments, which still has adequate space to increase. However, the undesirable side wings in the temporal profile of the self-compressed pulse are difficult to eliminate, mainly because high order dispersions of the medium are not compensated by plasma effect.

5. Conclusion

In summary, our numerical simulation shows that applying self-compression in multiple thin plates is a compact and effective method to produce few-cycle pulses which can be extracted with annular spatial filtering, by avoiding pulse splitting along the propagation axis. This method has also been proved in experiments, which could be a compact and reliable few-cycle pulse generation set-up with great potential to generate high power short pulses. Moreover,

through the utilization of conical emission, we realize continuous regulation of plasma density by moving the spatial filter along the radial direction. It is possible to provide an accurate control of plasma-induced negative dispersion. Finally, the pulse is compressed from 40 to 5.0 fs in numerical simulations, which may be potentially compressed even further with loose focusing and precise control of plasma density in each plate. The simulation results present a clear physical picture of the spatial self-compression method and how its parameters may be adjusted and controlled. This method has great potential in high-power few-cycle pulse generation as well as high-power attosecond pulse generation. Meanwhile corresponding experimental study has been done to verify our simulation results, and sub-10fs self-compressed pulses are obtained. We will optimize the experimental conditions such as increasing the focusing length and the size of the laser beam to avoid material damaging in the following works. Future works to increase the energy of the self-compressed pulses by reducing the radius of the hollow beam or matching the dispersion along the propagation axis are of great interest.

Funding. National Key Research and Development Program of China (2017YFB0405202); National Natural Science Foundation of China (61690221, 91850209).

Acknowledgments. We thank Tingting Xi of University of Chinese Academy of Sciences for helpful discussion in solving the propagation equation.

Disclosures. The authors declare no conflicts of interest.

Data availability. Data underlying the results presented in this paper may be obtained from the authors upon reasonable request.

References

1. I. G. Koprnikov, A. Suda, P. Wang, and K. Midorikawa, "Self-Compression of High-Intensity Femtosecond Optical Pulses and Spatiotemporal Soliton Generation," *Phys. Rev. Lett.* **84**(17), 3847–3850 (2000).
2. G. Stibenz, N. Zhavoronkov, and G. Steinmeyer, "Self-compression of millijoule pulses to 7.8 fs duration in a white-light filament," *Opt. Lett.* **31**(2), 274–276 (2006).
3. J. K. Ranka and A. L. Gaeta, "Breakdown of the slowly varying envelope approximation in the self-focusing of ultrashort pulses," *Opt. Lett.* **23**(7), 534–536 (1998).
4. S. Henz and J. Herrmann, "Self-channeling and pulse shortening of femtosecond pulses in multiphoton-ionized dispersive dielectric solids," *Phys. Rev. A* **59**(3), 2528–2531 (1999).
5. H. Liang, P. Kroger, R. Grynk, O. Novak, and K. H. Hong, "Three-octave-spanning supercontinuum generation and sub-two-cycle self-compression of mid-infrared filaments in dielectrics," *Opt. Lett.* **40**(6), 1069–1072 (2015).
6. M. L. Hemmer, M. Baudisch, A. Thai, A. Couairon, and J. Biegert, "Self-compression to sub-3-cycle duration of mid-infrared optical pulses in dielectrics," *Opt. Express* **21**(23), 28095–28102 (2013).
7. N. L. Wagner, E. A. Gibson, T. Popmintchev, I. P. Christov, M. M. Murnane, and H. C. Kapteyn, "Self-compression of ultrashort pulses through ionization-induced spatiotemporal reshaping," *Phys. Rev. Lett.* **93**(17), 173902 (2004).
8. L. Bergé and A. Couairon, "Gas-Induced Solitons," *Phys. Rev. Lett.* **86**(6), 1003–1006 (2001).
9. S. Skupin, G. Stibenz, L. Bergé, F. Lederer, T. Sokollik, M. Schnürer, N. Zhavoronkov, and G. Steinmeyer, "Self-compression by femtosecond pulse filamentation: Experiments versus numerical simulations," *Phys. Rev. E* **74**(5), 056604 (2006).
10. E. Goulielmakis, S. Koehler, B. Reiter, M. Schultze, A. J. Verhoef, E. E. Serebryannikov, A. M. Zheltikov, and F. Krausz, "Ultrabroadband, coherent light source based on self-channeling of few-cycle pulses in helium," *Opt. Lett.* **33**(13), 1407–1409 (2008).
11. P. A. Zhokhov and A. M. Zheltikov, "Attosecond Shock Waves," *Phys. Rev. Lett.* **110**(18), 183903 (2013).
12. C. Brée, I. Babushkin, U. Morgner, and A. Demircan, "Regularizing Aperiodic Cycles of Resonant Radiation in Filament Light Bullets," *Phys. Rev. Lett.* **118**(16), 163901 (2017).
13. H. Ward and L. Bergé, "Temporal shaping of femtosecond solitary pulses in photoionized media," *Phys. Rev. Lett.* **90**(5), 053901 (2003).
14. T. Balciunas, C. Fourcade-Dutin, G. Fan, T. Witting, A. A. Voronin, A. M. Zheltikov, F. Gerome, G. G. Paulus, A. Baltuska, and F. Benabid, "A strong-field driver in the single-cycle regime based on self-compression in a kagome fibre," *Nat. Commun.* **6**(1), 6117 (2015).
15. I. Babushkin, A. Tajalli, H. Sayinc, U. Morgner, G. Steinmeyer, and A. Demircan, "Simple route toward efficient frequency conversion for generation of fully coherent supercontinua in the mid-IR and UV range," *Light: Sci. Appl.* **6**(2), e16218 (2017).
16. A. A. Voronin and A. M. Zheltikov, "Sub-half-cycle field transients from shock-wave-assisted soliton self-compression," *Sci. Rep.* **10**(1), 12253 (2020).
17. J. C. Travers, T. F. Grigorieva, C. Brahm, and F. Belli, "High-energy pulse self-compression and ultraviolet generation through soliton dynamics in hollow capillary fibres," *Nat. Photonics* **13**(8), 547–554 (2019).

18. C. Brahms, F. Belli, and J. C. Travers, "Infrared attosecond field transients and UV to IR few-femtosecond pulses generated by high-energy soliton self-compression," *Phys. Rev. Res.* **2**(4), 043037 (2020).
19. A. Couairon, M. Franco, A. Mysyrowicz, J. Biegert, and U. Keller, "Pulse self-compression to the single-cycle limit by filamentation in a gas with a pressure gradient," *Opt. Lett.* **30**(19), 2657–2659 (2005).
20. J. Liu, X. W. Chen, J. S. Liu, Y. Zhu, Y. X. Leng, J. Dai, R. X. Li, and Z. Z. Xu, "Spectrum reshaping and pulse self-compression in normally dispersive media with negatively chirped femtosecond pulses," *Opt. Express* **14**(2), 979–987 (2006).
21. C. H. Lu, Y. J. Tsou, H. Y. Chen, B. H. Chen, Y. C. Cheng, S. D. Yang, M. C. Chen, C. C. Hsu, and A. H. Kung, "Generation of intense supercontinuum in condensed media," *Optica* **1**(6), 400–406 (2014).
22. P. He, Y. Liu, K. Zhao, H. Teng, X. He, P. Huang, H. Huang, S. Zhong, Y. Jiang, and S. Fang, "High-efficiency supercontinuum generation in solid thin plates at 0.1 TW level," *Opt. Lett.* **42**(3), 474–477 (2017).
23. O. G. Kosareva, V. P. Kandidov, A. Brodeur, C. Y. Chien, and S. L. Chin, "Conical emission from laser plasma interactions in the filamentation of powerful ultrashort laser pulses in air," *Opt. Lett.* **22**(17), 1332–1334 (1997).
24. F. Théberge, M. Châteauneuf, V. Ross, P. Mathieu, and J. Dubois, "Ultrabroadband conical emission generated from the ultraviolet up to the far-infrared during the optical filamentation in air," *Opt. Lett.* **33**(21), 2515–2517 (2008).
25. D. Faccio, M. A. Porras, A. Dubietis, F. Bragheri, A. Couairon, and P. D. Trapani, "Conical emission, pulse splitting and X-wave parametric amplification in nonlinear dynamics of ultrashort light pulses," *Phys. Rev. Lett.* **96**(19), 193901 (2006).
26. S. Trillo, C. Conti, P. D. Trapani, O. Jedrkiewicz, J. Trull, G. Valiulis, and G. Bellanca, "Colored conical emission by means of second-harmonic generation," *Opt. Lett.* **27**(16), 1451–1453 (2002).
27. F. Bragheri, D. Faccio, A. Couairon, A. Matijosius, and P. D. Trapani, "Conical-emission and shock-front dynamics in femtosecond laser-pulse filamentation," *Phys. Rev. A* **76**(2), 025801 (2007).
28. Z. X. Wu, H. B. Jiang, Q. Sun, H. Yang, and Q. H. Gong, "Filamentation and temporal reshaping of a femtosecond pulse in fused silica," *Phys. Rev. A* **68**(6), 063820 (2003).
29. L. Sudrie, A. Couairon, M. Franco, B. Lamouroux, and A. Mysyrowicz, "Femtosecond Laser-Induced Damage and Filamentary Propagation in Fused Silica," *Phys. Rev. Lett.* **89**(18), 186601 (2002).
30. Y. C. Cheng, C. H. Lu, Y. Y. Lin, and A. H. Kung, "Supercontinuum generation in a multi-plate medium," *Opt. Express* **24**(7), 7224–7231 (2016).
31. L. Bergé, S. Skupin, R. Nuter, J. Kasparian, and J. P. Wolf, "Ultrashort filaments of light in weakly ionized, optically transparent media," *Rep. Prog. Phys.* **70**(10), 1633–1713 (2007).
32. O. Shorokhov, A. Pukhov, and I. Kostyukov, "Self-Compression of Laser Pulses in Plasma," *Phys. Rev. Lett.* **91**(26), 265002 (2003).
33. R. Klas, A. Kirsche, M. Tschernajew, J. Rothhardt, and J. Limpert, "Annular beam driven high harmonic generation for high flux coherent XUV and soft X-ray radiation," *Opt. Express* **26**(15), 19318–19327 (2018).
34. M. Seidel, G. Arisholm, J. Brons, V. Pervak, and O. Pronin, "All solid-state spectral broadening: an average and peak power scalable method for compression of ultrashort pulses," *Opt. Express* **24**(9), 9412–9428 (2016).
35. J. E. Beetar, S. G. Mirzaei, and M. Chini, "Spectral broadening and pulse compression of a 400 μ J, 20 W Yb:KGW laser using a multi-plate medium," *Appl. Phys. Lett.* **112**(5), 051102 (2018).